Spectroscopic Study of Extracellular Polymeric Substances from *Bacillus subtilis*: Aqueous Chemistry and Adsorption Effects

Anselm Omoike and Jon Chorover*

Department of Soil, Water and Environmental Science, University of Arizona, Tucson, Arizona 85721-0038

Received November 7, 2003; Revised Manuscript Received March 3, 2004

Reactions at ionizable functional groups in extracellular polymeric substances (EPS) from *Bacillus subtilis* are found to affect aqueous phase conformation and adsorption to mineral surfaces. Characterization by HPSEC, XPS, and FTIR indicates a wide range in apparent molecular mass (0.57−128 kDa), with functional group composition depending on cell growth phase (exponential vs stationary) and location in suspension (free vs cell-bound). ATR-FTIR spectroscopy shows complexation and dissociation of protons on acidic functional groups that result in α-helical protein conformation at pH < 2.6 and random coil (unordered) conformation at higher pH (>6). EPS exhibit higher affinity for adsorption to α-FeOOH than amorphous SiO_2 because of surface charge effects. Increased amide II band intensity and an amide I band shift to higher frequency indicate changes in protein structure upon adsorption. Goethite-EPS spectra show emergent vibrations consistent with P−O−Fe bonding, which suggests a role of phosphodiester groups in the adsorption reaction.

Introduction

The partitioning and mobility of bacterial cells in aqueous environments between mineral or organic surfaces and the aqueous phase depends on the charge and hydrophobicity of the cell and available environmental surfaces, chemical bonding interactions, and solution chemistry.[1−5] Most bacterial cells exhibit a net negative surface charge that varies in magnitude with pH, because of ionization of acidic functional groups (e.g., carboxyl, hydroxyl, phosphate and amide) of cell surface lipopolysaccharides, teichoic acids and extracellular polymeric substances.[6−9] Mineral surfaces exhibit positive or negative charge depending on isomorphic substitutions and the Brönsted acidity of their surface hydroxyl groups.[10] Iron and Al (hydr)oxides may be positively charged at pH < 7 and negatively charged at pH > 7, whereas silica surfaces are negatively charged at pH > 2. Thus, bacterial adhesion to silica is enhanced by surface coatings of Al or Fe oxide and/or by increasing ionic strength to reduce electrostatic repulsion.[11] However, different bacterial cells of similar charge show significant differences in adhesion to surfaces,[12] which suggests an important role for molecular-scale interactions between cell and mineral surface functional groups.[5,13−14] These molecular-scale mechanisms remain unclear, partly because of the heterogeneity of cell surface macromolecules and also because information on adsorption affinities of individual macromolecular constituents and functional groups is lacking.

Bacterial extracellular polymeric substances (EPS) are a complex mixture of macromolecular polyelectrolytes including polysaccharides, proteins, and nucleic acids, each comprising variable molecular mass and structural properties.[15] In cell suspensions, EPS are distributed between the cell surface (i.e., capsular or cell-bound EPS), the aqueous phase (i.e., slime or free EPS), or a hydrated matrix in biofilm (biofilm EPS), with a composition that depends on growth phase and solution chemistry. This mixture mediates cell adhesion through interfacial processes including covalent or ionic bonding, dipole interactions, steric interactions, and hydrophobic association.[16−23] Components of free EPS may adsorb to mineral surfaces during "conditioning film" formation, prior to cell attachment. Therefore, both cell-bound and free EPS likely mediate surface interactions before biofilm formation.[24−30] Surface activity and conformation of EPS constituents depend on environmental factors. For example, the conformation of adsorbed protein depends on temperature, solution pH, electrolyte and macromolecule concentration, and adsorbent surface chemistry.[31−34]

Since EPS occurs as a complex mixture in aqueous environments, methods that are used to probe their physicochemical behavior should do so in the context of that mixture and in the presence of water. Attenuated total reflectance−Fourier transform infrared spectroscopy (ATR−FTIR) is a noninvasive, in-situ spectroscopic method that permits interrogation of functional group chemistry, conformational changes, and adsorption reactions in aqueous systems without disrupting intermolecular associations (e.g., protein−polysaccharide) that may be characteristic of EPS solutions. The objective of the present study was to examine the functionality, composition, and aqueous-surface reactivity of EPS extracted from the culture medium of a common gram-positive soil bacterium, *Bacillus subtilis* (ATCC 7003), grown to the exponential and stationary phases. The extracted EPS were purified and characterized by Fourier transform

* To whom correspondence should be addressed. Phone: (520) 626-5635. Fax: (520) 621-1647. E-mail: Chorover@cals.arizona.edu.

10.1021/bm034461z CCC: $27.50
Published on Web 04/23/2004

infrared spectroscopy (FTIR), X-ray photoelectron spectroscopy (XPS), and high performance size exclusion chromatography (HPSEC). ATR-FTIR spectroscopy was then used as an in-situ technique to probe the influence of aqueous solution chemistry (pH and ionic strength) on ionization of EPS, to assess conformational changes of constituent proteins, and to elucidate sorptive interactions with colloidal goethite (α-FeOOH) and amorphous silica (SiO_2,am).

Experimental Section

All solutions were prepared using ultrapure (Milli-Q UV-plus) water and analytical grade chemicals. The pH of all aqueous solutions and oxide suspensions was adjusted using NaOH or HCl, and the final ionic strength (10−100 mM) was adjusted by addition of NaCl. All experiments were conducted in duplicate at 23 ± 1 °C. Deuterium oxide (D_2O, 99.9%) was purchased from Cambridge Isotope Laboratories, Inc.

EPS Extraction. The test bacterium, *B. subtilis* (ATCC7003), was cultivated aerobically in Luria broth (LB) at 30 °C and 150 rpm to exponential (4 h) and stationary (24 h) growth phases in 250 mL flasks. For extraction of EPS, we used the protocol reported by de Brouwer et al.[35] except that the extracting solvent was 100 mM NaCl (pH 7.0) instead of distilled water.

Cells were harvested by centrifugation (5000 g, 15 min, 4 °C) and washed once by resuspension in 100 mM NaCl solution at pH 7.0. Washed cells were pelleted by centrifugation and re-suspended in EPS extracting solution (100 mM NaCl, pH 7.0). The cells were extracted by shaking for 1 h at 30 °C in a water bath at 100 reciprocations per min, and the supernatant solution was recovered by centrifugation (5000 g, 30 min, 4 °C). Supernatant solutions from the cell culture (LB) and cell extracting (NaCl) solutions were centrifuged (12 000 g, 30 min, 4 °C) to remove residual cells. The "free" (from growth medium) and "cell-bound" (from NaCl solution) EPS were then precipitated by reaction with 3 volumes of cold reagent-grade ethanol, and the suspension was stored at −20 °C for 18 h. The crude EPS was separated from the supernatant solution by centrifugation (12 000 g, 30 min and 4 °C). The pellet obtained was dissolved in ultrapure (Milli-Q) water and dialyzed against the same using Spectra/Por 7 regenerated cellulose (RC) membranes (1000 MWCO from Spectrum) to remove ethanol and entrained media residues. After dialysis for 72 h against two changes of Milli-Q water per day, the solution was freeze-dried.

Mineral Adsorbents. Goethite (α-FeOOH) and amorphous silica (SiO_2 am) were used as model adsorbents because they are common to soils and aquatic systems and they exhibit variable surface charge that is positive (goethite) or negative (silica) at circumneutral soil pH.[10] Goethite was synthesized from $Fe(NO_3)_3$ using the method of Atkinson et al.[36] The precipitate was washed repeatedly with 1 mM HCl until the pH of the supernatant solution was 4.0, and it was then rinsed with Milli-Q water until the conductivity was equal to that of the input water and finally freeze-dried. The specific surface area of goethite (measured by multipoint N_2−BET) was 44.4 $m^2\ g^{-1}$. Amorphous silica was purchased from Degussa (Sipernat 350, 50 $m^2\ g^{-1}$) and washed three times with 10 mM NaCl solution, prior to rinsing with Milli-Q water until the conductivity of the supernatant solution was 0.055 dS m^{-1}. Milli-Q water and background electrolyte (10 mM NaCl) were purged with N_2(g) in preparation and dilution of oxide stock suspensions (25 g kg^{-1}).

pH/pD Measurements. A Symphony benchtop pH/ISE/Conductivity meter (VWR, SR601C) was used for all pH/pD measurements. The pD was measured with a standard pH electrode and the value was corrected using pD = pH + 0.4.[37]

Quantitation of Polysaccharides, Proteins, and DNA. Carbohydrates were assayed by the phenol-sulfuric acid method of Dubios et al.[38] EPS solutions were prepared at concentrations of 1 mg mL^{-1}, and 0.5 mL was mixed with 1 mL of 5% (w/v) phenol in thick walled glass test tubes. After mixing, 2.5 mL of concentrated H_2SO_4 were added to each tube with slight shaking. Samples were left to stand for 10 min and then heated at 30 °C for 20 min. Sugar concentration was measured against glucose standards by absorbance at 490 nm. Proteins and DNA were assayed by Lowry method[39] (SIGMA, St Louis, MO) and the fluorescent dye bisBENZIMIDE (Hoechst 33258) assay (SIGMA, St Louis, MO), respectively, following the manufacturer's protocol. Bovine serum albumin (BSA) and calf thymus DNA were used as calibration standards. The DNA assay is optimized for measurement of double-stranded DNA in relatively pure samples; it is known to be less sensitive to RNA and single-stranded DNA and thus likely provides systematically low estimates in the presence of other EPS biopolymers.

Apparent Molar Mass. High performance size exclusion chromatography (HPSEC) was used to index molecular weight distributions of EPS in aqueous solutions. The HPSEC system comprised a Waters high performance liquid chromatography (HPLC) unit equipped with a 600 pump, a 717 plus autosampler, and 996 photodiode array and a 410 differential refractometer detectors in series. Two stainless steel (8 × 300 mm) SEC columns (HEMA Bio 100 Å and 1000 Å, PSS Polymer Standards-USA, Silver Spring, MD), with guard columns, were connected in series to enable separation across the full size range of isolated EPS in a mobile phase of 10 mM NaCl (pH 6.0). Freeze-dried EPS was dissolved in the mobile phase to give a concentration of 3.0 mg mL^{-1}.

Calibration of molar mass to retention time was accomplished using pullulan standards (2.0 mg mL^{-1}) of nominal molecular masses 5.8, 12.2, 23.7, 48.0, 212, and 380 kDa and polydispersity values less than 1.2 (Polymer Laboratories, Silver Spring MD). Pullulan standards were selected because they have structural, mass range, and charge distribution properties representative of some bacterial polysaccharides. Numerous microbial polysaccharides consist of glucose units linked by α[1 → 3], α[1 → 4], and α[1 → 6] or some combination thereof.[40,41] Although dextran (α[1 → 6] glycosidic linkages) and pullulan (α[1 → 4] and α[1 → 6] linkages) both occur in EPS and have been widely used as HPSEC biopolymer standards for biopolymers, we

selected relatively monodisperse pullulan because of its greater stability and structure.[42] Monomeric glucose was included in the calibration. The injection volume and flow rate for all samples and standards were 100 μL and 1.0 mL min^{-1}, respectively. Weight- (M_w) and number- (M_n) averaged molar mass values were calculated in the Empower software program (Waters Inc., Medford, MA) according to

$$M_w = \sum_{i=1}^{N} h_i(M_i) / \sum_{i=1}^{N} h_i \quad (1)$$

$$M_n = \sum_{i=1}^{N} h_i / \sum_{i=1}^{N} (h_i/M_i) \quad (2)$$

where h_i and M_i are the height and molecular mass, respectively, of the sample HPSEC curve eluted at volume i.

X-ray Photoelectron Spectroscopy. XPS measurements were made on a KRATOS AXIS 165 Ultra Photoelectron Spectrometer operated at 15 KV and 20 mA using Al Kα (1486.6 eV) radiation. The takeoff angle, defined as the angle between the substrate normal and the detector, was fixed at 90°. Substrates were mounted on standard sample studs by means of double sided adhesive tape. Binding energies were calibrated using the C (1s) peak (284.6 eV). Analysis consisted of a broad survey scan (20.0 eV pass energy) for major element composition and a high-resolution scan (80.0 eV pass energy) for component speciation. All of the XPS analyses were performed in duplicate (two independent samples of each type of EPS analyzed at different times).

Total C and N. 1 mg of EPS was dissolved in 10 mL of water acidified with HCl to pH 2 and the total organic C and N concentrations were determined by high-temperature combustion and infrared detection of CO_2 and NO using a Shimadzu TOC−V CSH TOC/TN analyzer (Columbia, MD). Potassium hydrogen phthalate [$(HO_2C)_2(COOK)$-C_6H_4] and potassium nitrate (KNO_3) were used as standards for DOC and TN, respectively.

Infrared Spectroscopy. All spectra were acquired using a Nicolet Magna 560 FTIR spectrometer at 4.0 cm^{-1} resolution with 350−500 scans. For collection of diffuse reflectance FTIR (DRIFT) spectra, powdered analyte was folded into IR grade KBr powder at a mass ratio of 1:200. The sample was transferred to a 4 mm diameter cup and the surface was leveled. Samples were mounted into a Spectra Tech baseline diffuse reflectance cell fitted to the sampling compartment of the spectrometer. All DRIFT spectra were corrected for a KBr background.

ATR−FTIR measurements were obtained on aqueous phase samples of free EPS (10 mg mL^{-1}) using a trough-style sample holder with a Ge internal reflection element (IRE) (70 mm × 10 mm × 3 mm) subjected to a nominal incident beam angle of 45°, yielding 12 internal reflections at the sample surface. For ATR studies of adsorption, thin films of colloidal goethite and silica were deposited on the IRE surface by evenly dispensing 500 μL of the sonicated colloidal stock suspension (25 g kg^{-1} suspension, 10 mM NaCl; pH 6.0) over the Ge crystal. The spectrum of the suspension was recorded after 30 min. The trough was removed from the sampling accessory, and the slurry was allowed to dry in a vacuum oven (19 h) at room temperature. The spectrum of the dried oxide was recorded. Background electrolyte (500 μL of 10mM NaCl) was added to the dried film, and the liquid was carefully drained out in order to remove unattached particles, rehydrate the oxides, and prevent EPS protein denaturation at the air/water interface. The spectrum of the rehydrated oxide was obtained. An aliquot of the EPS stock solution (500 μL) was then introduced, and the sample spectra were recorded as a function of time (8, 15, 30, 60, and 120 min.). All ATR spectra use the clean Ge crystal as background.

Table 1. Chemical Constituents of Free and Bound EPS from *Bacillus subtilis*

	EPS (growth phase)		
constituents	free (exponential)	bound (stationary)	free (stationary)
carbohydrate	46.34 ± 0.21	42.89 ± 0.1	28.06 ± 0.14
protein	20.60 ± 0.49	26.46 ± 0.25	32.89 ± 0.80

Results and Discussion

Under the growth conditions employed, *B. subtilis* produced a much higher quantity of free (420 mg L^{-1}) relative to cell-bound (13.1 mg L^{-1}) EPS in the stationary growth phase. Standard quantification of proteins and carbohydrates indicated that these biomolecular classes constitute the majority of EPS by mass, with protein increasing relative to carbohydrate in free EPS as growth stage proceeds from the exponential to stationary phase (Table 1). Because of the low density of cells produced in the exponential growth phase, the mass of cell-bound EPS was insufficient for analysis.

Molecular Size Distribution. The size distribution of EPS macromolecules was examined using HPSEC coupled with UV absorbance and refractive index (RI) detection. Whereas UV absorbance detects conjugated C−C bonded structures, the refractive index increment is measurable on the entire eluate. In the present work, UV and RI detection in series provided complementary information regarding molar mass distribution of the mixture comprising UV nonabsorbing (carbohydrate) and absorbing (protein, nucleic acid) constituents. The photodiode-array (PDA) detector provides the additional capability to obtain a full UV spectrum on each chromatographic peak. RI chromatograms of solutions containing 1, 3, and 6 mg mL^{-1} of EPS in 10 mM NaCl at pH 6.0 indicate four peaks with elution times of 14.24, 16.62, 20.60, and 24.66 min (Figure 1). Weight and number averaged molecular weights (M_w and M_n) are indicated in Table 2. The peak with elution time of 24.66 min was outside of the low mass calibration limit. Peak area ratios were found to be independent of aqueous phase concentration for the range 1−6 mg mL^{-1}, and polydispersity values for each peak were generally < 1.5. Subsequent HPSEC measurements employed 3 mg mL^{-1} EPS. Representative UV (280 nm) and RI chromatograms show the size distributions of chromophores and bulk biopolymeric constituents, respectively (Figure 2a). Conjunctive use of the detectors indicates that the RI peaks may be further decomposed into smaller pop-

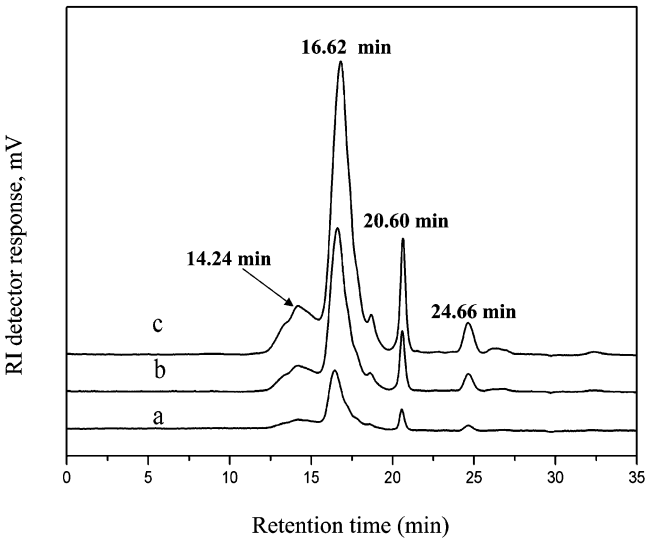

Figure 1. HPSEC chromatograms at three different EPS concentrations: (a) 1, (b) 3, and (c) 6 mg/mL.

Table 2. Apparent Molecular Mass Distribution Data for Three Concentrations of EPS (Free-Stationary Phase) from Pullulan Standards and Refractive Index HPSEC Detection (10 mM NaCl Solution and pH 6)

conc	molecular weight, kDa		polydispersity	
mg/mL	M_n	M_w	M_w/M_n	area (%)
		14.24 min. peak		
1.0	83.1	123.2	1.48	20.13 ± 4.33
3.0	89.8	132.7	1.48	16.68 ± 0.85
6.0	85.8	128.5	1.50	16.87 ± 0.61
	(86.2 ± 3.4)	(128.1 ± 4.8)	(1.49 ± 0.01)	
		16.62 min. peak		
1.0	8.2	12.8	1.57	68.83 ± 3.13
3.0	8.7	12.4	1.43	71.47 ± 1.46
6.0	8.9	11.6	1.30	70.46 ± 1.33
	(8.6 ± 0.4)	(12.2 ± 0.6)	(1.43 ± 0.13)	
		20.60 min. peak		
1.0	0.56	0.58	1.033	7.77 ± 0.84
3.0	0.55	0.57	1.032	8.13 ± 0.60
6.0	0.54	0.56	1.034	8.58 ± 0.78
	(0.55 ± 0.01)	(0.57 ± 0.01)	(1.033 ± 0.001)	
		24.66 min. peak[a]		

[a] Low molecular mass compound outside the calibration range.

ulations of variable-sized macromolecules. For example, the largest peak (16.62 min) in the RI profile is partially resolved into four UV chromatogram peaks (Figure 2a). When the full photodiode array spectrum for each of these four peaks is expanded (Figure 2b), it is apparent that even a single RI peak (16.62 min peak) comprises compositionally distinct macromolecules with unique λ_{max} values and UV spectral shapes. The UV absorbing macromolecules are proteins and nucleic acids, whereas the other constituents are predominantly polysaccharides. Proteins typically exhibit local λ_{max} at ca. 280 nm, whereas nucleic acids show λ_{max} at ca. 260 nm. The absorbance ratio at these two wavelengths can be used as an index of the relative concentrations of these biomolecular classes. Thus, peaks eluting at 15 and 15.8 min are characteristic of protein, whereas peaks eluting at 16.64 and 17.4 min are characteristic of nucleic acid bases and aromatic amino acids. When plotted as a function of elution time, the ratio A_{260nm}/A_{280nm} suggests that peaks eluting at 16.64, 17.4, and 23.95 are predominantly nucleic acids (Figure 2c). These results emphasize the fact that trends in spectroscopic properties (discussed below) must be considered in light of the essential heterogeneity of the EPS mixture.

XPS. X-ray photoelectron spectra over the energy range of 0−1200 eV (1.0 eV step-size) show that both "free" and "cell-bound" EPS comprise comparable elemental composition (Figure 3) albeit with different mass fractions (Table 3). The atomic composition of EPS, estimated from integrating the core level peaks C 1s, O 1s, N 1s, and P 2p, indicate ca. 61% C, 30% O, 8% N, and 1% P, with some variability depending upon source (Table 3). Similar mass fractions of C, O, N, and P (60.7, 30.9, 7.3, and 0.1%, respectively) were reported for EPS produced by a sulfate-reducing bacterial culture.[43] The Si peak is most likely derived from glassware used in the extraction protocol. The N (1s) line with a binding energy of 399 eV is consistent with N in amine or amide groups (RHN−C═O) of proteins.[44−46] In comparison, our wet chemical analysis of EPS carbon by high-temperature combustion and infrared detection of CO_2 indicates 28.9 ± 0.16% C for free EPS and 37.85 ± 0.26% C for cell-bound EPS at the stationary growth phase. The overestimate of C in XPS results is most likely attributable to adventitious hydrocarbon moieties [C (C, H)] resulting from preexposure of the sample to air and the XPS vacuum chamber, as reported previously.[43] It is also possible that XPS, a surface-sensitive technique, is detecting a higher C concentration at the surface, relative to bulk, of EPS molecules in the chamber.

XPS peaks pertaining to C and O were scanned at high resolution (0.1 eV step-size) and deconvoluted to assess the local chemical environment of these elements. All samples indicate the presence of four C(1s) (Figure 4) and two O(1s) environments (Figure 5). Peak integration results are included in Table 3. The peak pertaining to C singly bonded to N or O, which is attributed to alcohol, amine, or amide (286.2 ± 0.42 eV), is larger in free relative to bound EPS, whereas C and H bonded C is more prevalent in bound EPS (Figure 4 and Table 3). Fitted O(1s) spectra conform to these trends in that the contribution of alcohols (C-OH), hemiacetal and acetal (C-O-C-O-C) groups (532.2 ± 0.42 eV) is higher in free relative to bound EPS. The inverse is true for the second O(1s) component located at 531.0 ± 0.35 eV (Figure 5 and Table 3), which corresponds to O double bonded to C (C═O) as in carboxylic acid, carboxylate, carbonyl, or amide. The values we obtained for C−(O, N)/C (0.337 and 0.314 for free and bound EPS respectively, Table 3) are higher than those reported for proteins (0.26−0.293) but lower than those reported for polysaccharides (0.833).[47−50] Similarly, (C═O)/C + (O−C−O)/C values for free and bound EPS (0.144 and 0.141, respectively) are close to those reported for polysaccharides (0.167) and lower than those for proteins (0.225−0.279). Atomic ratios N/C, O/C, and P/C are higher for bound EPS, whereas N/P is higher in free EPS (Table 3). These atomic ratios obtained for free and cell-bound EPS are comparable to XPS ratios reported for bacterial surfaces.[47−50]

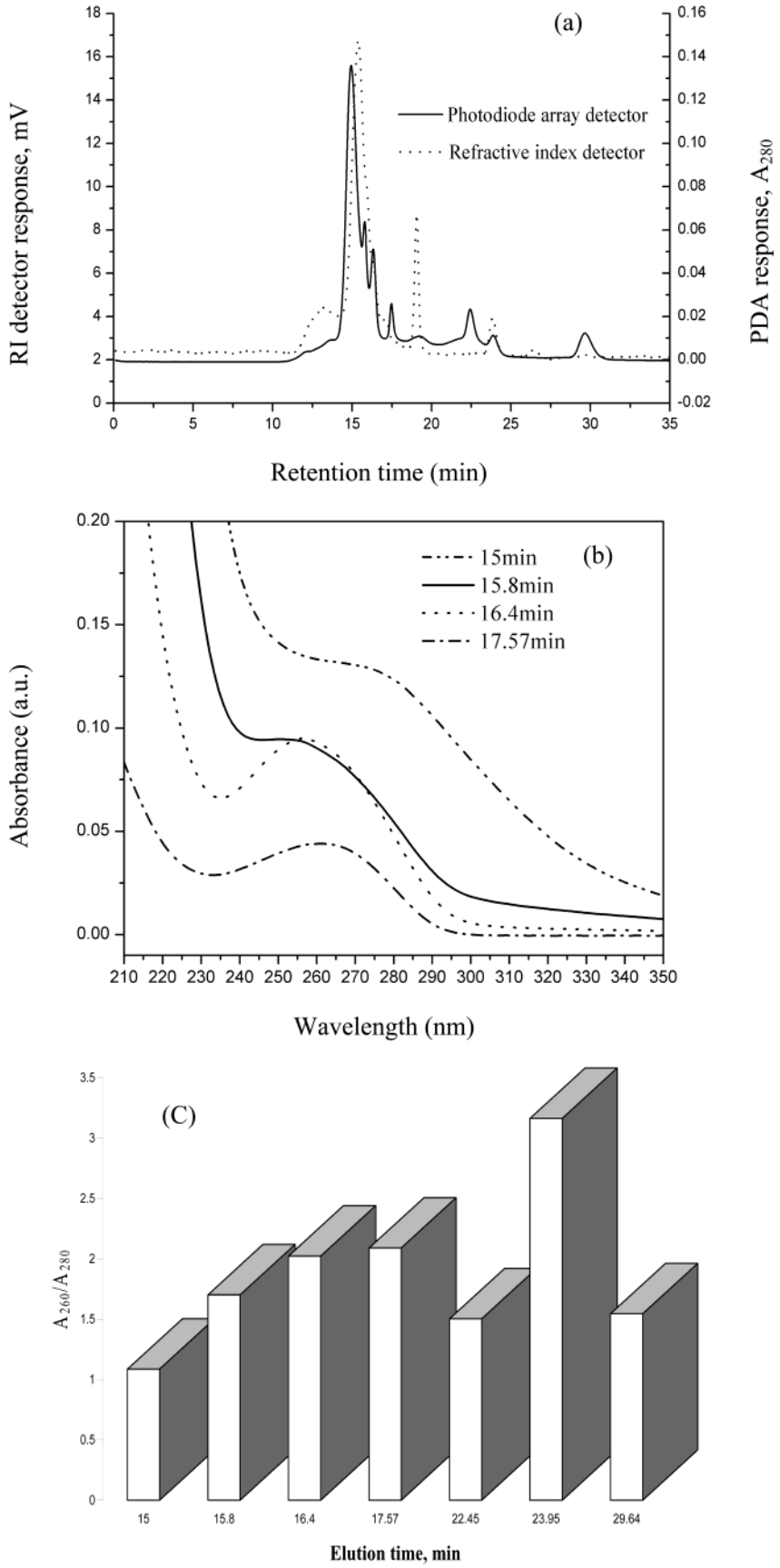

Figure 2. (a) Overlaid simultaneous RI and UV absorbance detection of HPSEC chromatogram for 3.12 mg/mL EPS solution (free-stationary) in 10 mM and pH 6. (b) Diode-array spectra of various UV-absorbing constituents that elute during the single RI chromatogram peak (15−18 min) for 3.12 mg/mL EPS solution (10 mM NaCl and pH 6). (c) A_{260nm}/A_{280nm} of the UV-absorbing fractions in the UV absorbance detection of HPSEC chromatogram of EPS as a function of elution time (3.12 mg/mL EPS solution in 10 mM and pH 6.)

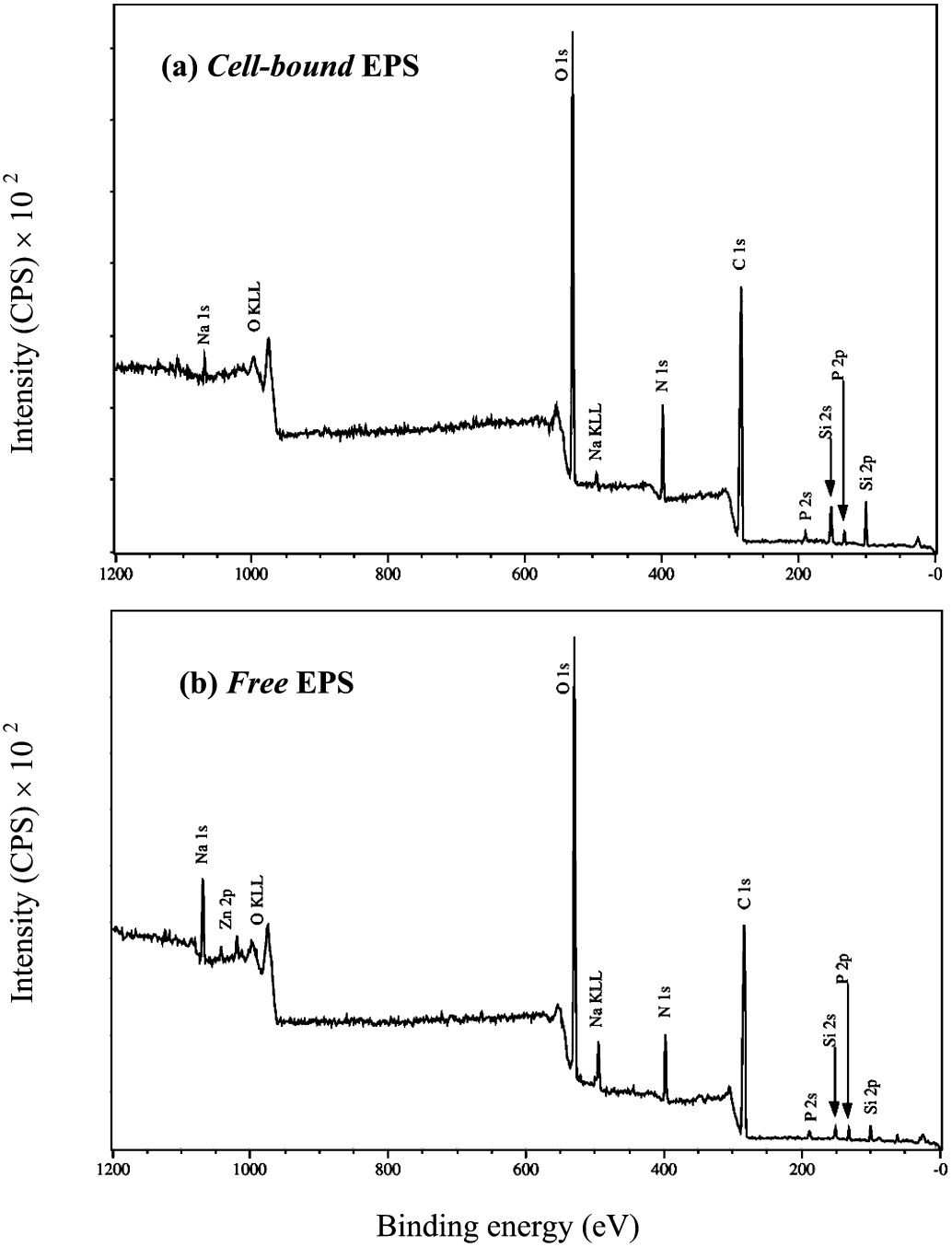

Figure 3. X-ray photoelectron low resolution spectra of (a) cell-bound and (b) free EPS.

DRIFT Spectra. Diffuse reflectance infrared Fourier transform (DRIFT) spectra indicate structural differences between bound and free EPS and also effects of growth stage (exponential versus stationary) (Figure 6). Band assignments[51−54] are provided in Table 4. All sample spectra show protein-specific bands (amide I and amide II) as well as those pertaining to polysaccharides and nucleic acids. The amide I band (1600−1700 cm^{-1}) originates predominantly from the C═O stretching vibrations of peptide groups in proteins, whereas the amide II band (1500−1600 cm^{-1}) includes N−H bending and C−N stretching vibrations. The band at 1400 cm^{-1} is due to symmetric carboxylate stretching. The asymmetric COO^- stretching vibration overlaps with the broad amide bands and is not distinguished in the spectra. All samples exhibit a peak in the region 1221−1241 cm^{-1} indicative of asymmetric PO_2^- stretching of phosphodiesters. This peak is shifted down in frequency (20 cm^{-1}) and increased in intensity for cell-bound (Figure 6 spectrum a) relative to free (Figure 6 spectrum b) EPS. Shifts associated with this band have been related to the hydration level of the group[55] and also to phosphate-sugar interaction.[56] However, ab initio modeling of phospholipids suggest that ester bond rotation of phosphate can induce the same frequency changes as hydration.[57] The C═O stretching vibration of esters (1743 cm^{-1}) is observed in cell-bound (Figure 6 spectrum a) but not in free EPS (Figure 6 spectrum b), suggesting that the peak at 288 eV in XPS spectra of free EPS is largely due to O−C−O of polysaccharides (Table 3). Both carbohydrates and nucleic acids give rise to the broad complex peak at 900−1200 cm^{-1} through C−O

Table 3. Binding Energies (eV) and Assignment/Quantitation of XPS Spectral Bands. Atomic Fractions for Elemental Composition Obtained from Low Resolution Data and High Resolution Spectra Used for Quantitation of Functional Group Composition[a]

element/elemental ratios	free EPS		bound EPS		
	peak (eV)	atomic (%)	peak (eV)	atomic (%)	assignments
C_{1s}	284.6 ± 0.21	46.05 ± 4.03	284.6 ± 0.42	51.05 ± 6.29	C−(C,H)
C_{1s}	286.2 ± 0.28	37.3 ± 2.12	286.2 ± 0.42	31.35 ± 5.02	C−(O, N)
C_{1s}	287.9 ± 0.28	14.4 ± 2.26	287.9 ± 0.42	14.1 ± 1.56	C═O + O−C−O
C_{1s}	288.9 ± 0.21	2.2 ± 0.42	288.9 ± 0.49	3.5 ± 0.14	O═C−OH
total C	284.6 ± 0.14	61.27 ± 0.61	284.7 ± 0.42	60.64 ± 0.78	
O_{1s}	531.0 ± 0.35	34.4 ± 4.53	531.3 ± 0.21	49 ± 7.35	O═C
O_{1s}	532.2 ± 0.21	65.6 ± 4.53	532.2 ± 0.42	55.5 ± 0.99	C−OH; C−O−C
total O	532.0 ± 0.28	31.47 ± 0.35	531.7 ± 0.35	28.44 ±0.20	
total N	399.7 ± 0.21	6.12 ± 0.28	399.6 ± 0.42	9.20 ± 0.32	
total P	133.4 ± 0.35	1.15 ± 0.01	133.5 ± 0.28	1.32 ± 0.08	
N/C	0.104 ± 0.0055		0.146 ± 0.0054		
O/C	0.507 ± 0.0076		0.549 ± 0.0080		
P/C	0.019 ± 0.0003		0.047 ± 0.0029		
N/P	5.530 ± 0.258		3.111 ± 0.217		

[a] Mean values ± standard deviations for duplicate samples are shown.

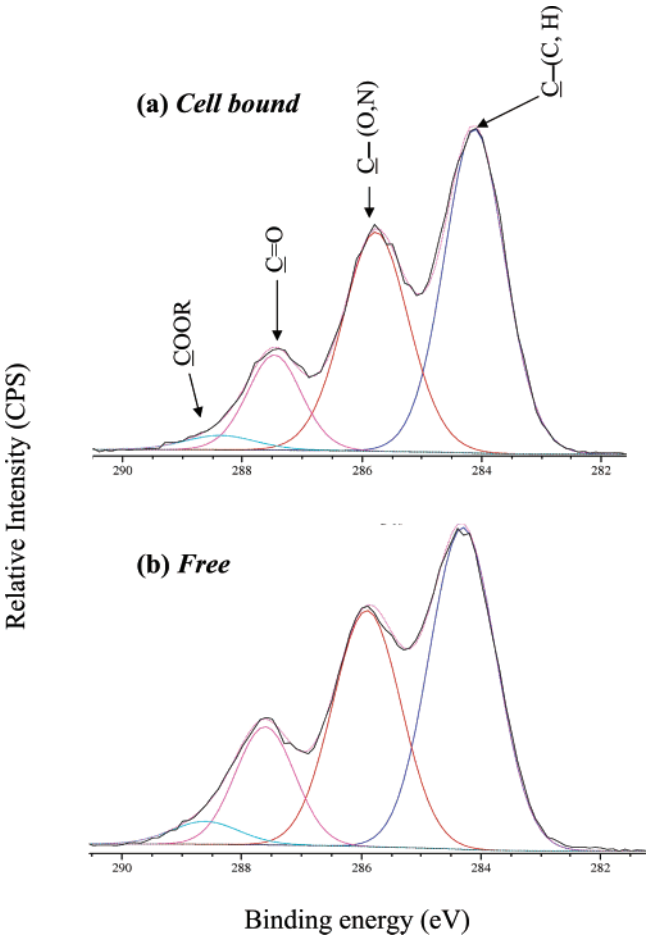

Figure 4. X-ray photoelectron high-resolution C 1s spectra of (a) cell-bound and (b) free EPS.

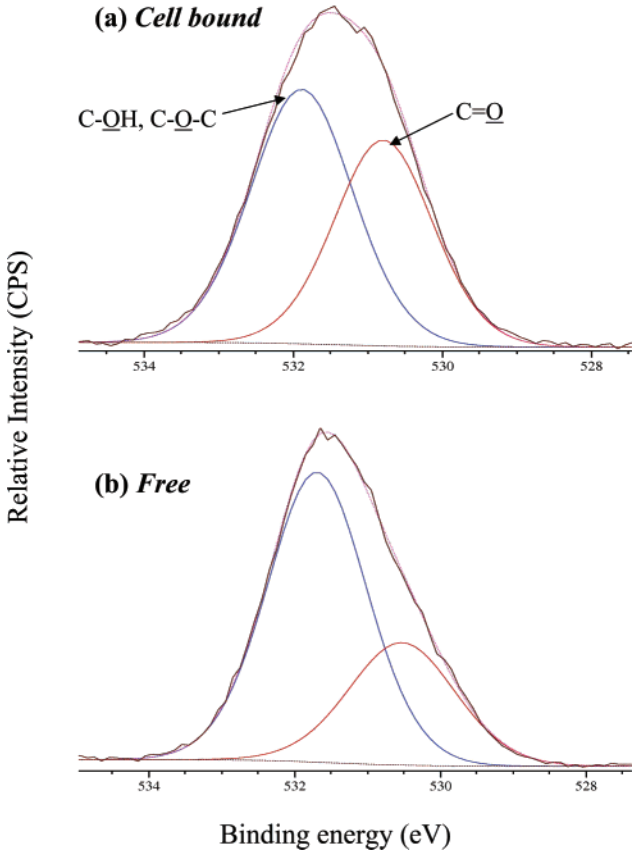

Figure 5. X-ray photoelectron high-resolution O 1s spectra of (a) cell-bound and (b) free EPS.

stretching vibrations of polysaccharides and the phosphodiester backbone of DNA/RNA.

Consistent with XPS results, the DRIFT data indicate that, relative to free EPS, the bound material contains a higher concentration of phosphodiester groups and/or phosphorylated proteins (1240 and 970 cm^{-1}) as well as C═O moieties (carboxylic acids, carboxylates, esters, carboxyl, or amides), but less polysaccharide functionality (1150−1000 cm^{-1}) [(C−(O,N); C-OH + C-O-C)]. Wet chemical analysis indicated that double-stranded DNA (a source of phosphodiester functionality) constituted 0.244 ± 0.036 and 1.903 ± 0.003% by mass of free and bound stationary-phase EPS, respectively. This is likely a significant underestimate of total nucleic acid concentration given that only double-stranded DNA is measured (single strands and RNA are excluded) and even that measurement can be compromised by the presence of proteins and polysaccharides. The greater polarity of O-containing polysaccharides likely contributes to their higher water solubility and prevalence in free EPS. In contrast, although the XPS data indicate a higher N concentration for bound EPS, the amide I and II band intensities are substantially greater for the free EPS (Figure 7b). Wet chemical analysis indicates 8.03 ± 0.62 and 3.71± 0.41% N for free and bound stationary phase EPS, in qualitative agreement with the DRIFT spectra. Similarly, proteins constituted 32.89 ± 0.80 and 26.46 ± 0.25% of free and bound stationary phase EPS mass, respectively. Growth phase

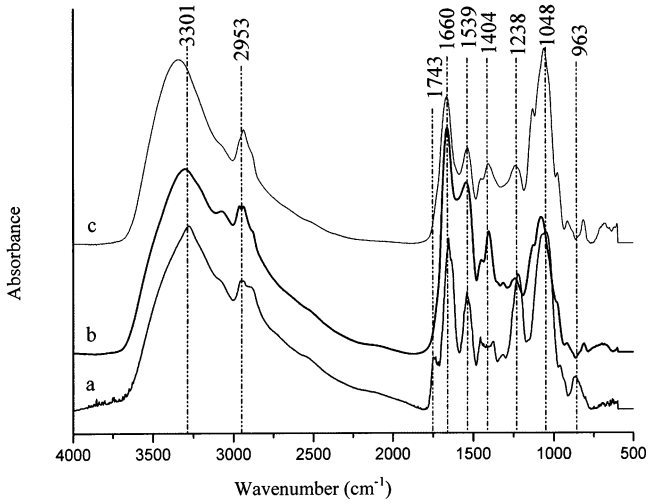

Figure 6. DRIFT spectra of EPS: (a) cell-bound/stationary growth phase, (b) free/stationary growth phase, and (c) free/exponential growth phase.

effects are also apparent; polysaccharide (1150−1000 cm^{-1}) band intensities of free EPS are greatest during exponential growth (Figure 6 spectrum c), whereas protein bands (1652−1548 cm^{-1}) are enhanced during stationary growth (Figure 6 spectrum b). Wet chemical analyses are in agreement with these FTIR data in respect to the predominance of carbohydrate during exponential growth and of protein at the stationary phase in free EPS (Table 1).

ATR-FTIR Spectra of EPS in Aqueous Solution

Spectra of free EPS suspended in 10 mM NaCl solution over the pH range 2.6−9.0 indicate progressive H^+ dissociation of carboxylic groups (Figure 7a). At pH 2.6, a shoulder at 1714 cm^{-1} is observed, corresponding to C═O stretching of protonated −COOH groups,[58,59] and this band disappears by pH 6.1 as a result of dissociation. Over the same pH range, the amide I band shifts from 1652 to 1644 cm^{-1}, and a new band corresponding to symmetric stretching of carboxylate ($-COO^-$) anion emerges at 1402 cm^{-1}.

Bands in the frequency range 900−1200 cm^{-1} result from bond vibrations of polysaccharides as well as DNA/RNA. At pH 9.0, a broad complex band is centered at 1088 cm^{-1} and a very weak band is at 1250 cm^{-1}. These bands are in the range for symmetric and asymmetric PO_2^- stretching, respectively, as well as carbohydrate O−H groups. With decreasing pH, the two bands shift to lower frequency and higher intensity (particularly the 1200−1250 cm^{-1} band), indicative of proton complexation of phosphate groups in the EPS. At pH values of 9, 6, and 2, the broad band (including the phosphate symmetric stretch) is centered at 1088, 1080, and 1076 cm^{-1} respectively. Similar peak shift to lower wavenumber with decreasing pH was reported during studies on protonation of aminomethylphosphonic acid (AMPA),[60] of glyphosate,[61] and of phosphate on the surface of goethite.[62] For example, in AMPA, the phosphate symmetric stretching bands at pH values of 9.7, 7.3, 5.3, and 2.1 were centered at 1089, 1091, 1080, and 1078 cm^{-1} respectively. Since the intensity of the 1275−1200 cm^{-1} band (asymmetric PO_2^- stretch) reflects the extent of H-bonding,[63]

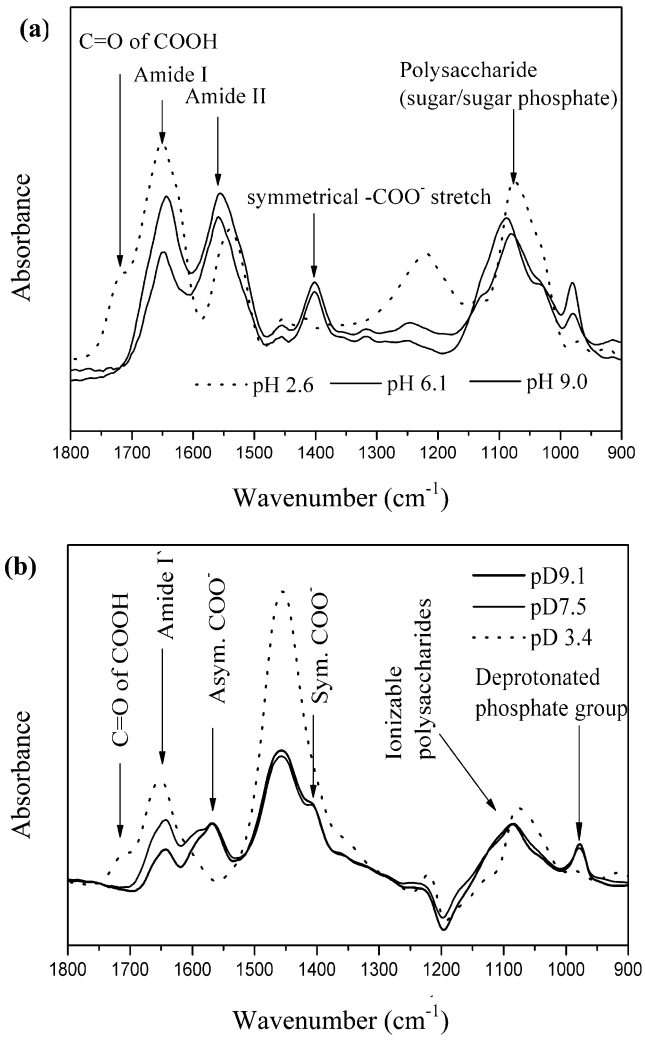

Figure 7. (a) Effect of solution pH and (b) pD on ATR-FTIR spectra of EPS (free/stationary growth phase) in 10 mM NaCl (10 mg EPS mL^{-1} and pD 3.4−9.1).

reduced intensity at higher pH is consistent with deprotonation and subsequent weakening of intra- or intermolecular H-bonds, which likely also influence macromolecular conformation. Changes in the C−OH bending vibration may also contribute to this pH effect (Table 4); decreased intensity of the 1080 cm^{-1} band with increasing pH may be attributed partially to dissociation of carboxylic and carbohydrate O−H groups, with a resultant decrease in H-bonded structure.

ATR-FTIR Spectra of EPS in D_2O. The amide I (1600−1700 cm^{-1}) and amide II (1500−1600 cm^{-1}) bands contain information on structural properties of EPS proteins, with the amide I band being most sensitive to conformational effects.[64−74] Bands at 1695−1660 and 1637−1613 cm^{-1} have been assigned to β-sheet or β-turns, 1660−1650 cm^{-1} to α-helical conformation, and 1650−1640 cm^{-1} to random coil (unordered) conformation.[65,69−71] Since the deformation of water (1640 cm^{-1}) obscures the amide I band and also overlaps with asymmetric stretching of carboxyl (1550 cm^{-1}), we acquired ATR-FTIR spectra of EPS in D_2O under comparable acid−base and ionic strength conditions (Figure 7b). The amide II band shifts to lower wavenumber (from 1542 cm^{-1} to 1456 cm^{-1}) due to H → D exchange of amide protons.[70] The D_2O spectra show ionization (pD) effects complementary to those observed in water. The deuterated

Table 4. Band Assignments for FTIR Spectra of Free and Bound EPS

vibration frequencies (cm^{-1})			
"bound" EPS (24 h)	"free" EPS (24 h)	"free" EPS (4 h)	band assignments[48−51]
3278	3301	3344	O−H stretching (hydrogen-bonded) N−H stretching (Secondary amides)
2953	2963	2936	CH stretching (CH_2 and CH_3 groups)
	2938		
1743			C═O stretching (esters)
1654	1660	1663	C═O stretching in secondary amides (amide I)
1539	1544	1535	N−H deformation and C−N stretching in −CO−NH− of proteins (amide II)
1455	1449	1451	symmetrical deformations of CH_2, C−OH deformations
1379	1404	1407	C═O of COO^- groups, symmetrical stretching
1221	1242	1238	asymmetric stretching P═O of phosphodiester backbone of nucleic acid or phosphorylated proteins
	1127	1129	O−H deformation, C−O stretching, ring vibrations of
1048	1078	1059	polysaccharides C−O−C and C−O−P
963	920	977	asymmetric ester O−P−O stretching modes from nucleic acids

carboxyl group is present at pD 3.4 (shoulder near 1714 cm^{-1}), but disappears at higher pD, concurrent with the emergence of asymmetric carboxylate ($-COO^-$) stretching at 1582 cm^{-1}. In D_2O, unlike in water, asymmetric $-COO^-$ is not masked by the amide II band. The decrease in wavenumber for the amide I band (denoted amide I′ for the D_2O system) with increasing pD confirms pH-dependent conformational changes of EPS protein. The data in Figure 7 indicate α-helical conformation at low pH and pD < 6 (amide I/I′ bands between 1660 and 1650 cm^{-1}) and random coil (unordered) conformation at high pH and pD > 6 (amide I/I′ bands between 1650 and 1640 cm^{-1}).[65,69−71]

Effects of Ionic Strength. In addition to proton complexation reactions at amide, carboxylic, and phosphate groups, conformational changes may result from nonlocalized screening of charged functional groups by adsorbed or aqueous phase background ions. To test for this effect, which should increase with solution ionic strength, we collected ATR spectra of EPS in pure water, 10 mM NaCl, and 100 mM NaCl at pH 6 (Figure 8a). Changes in band intensity likely reflect Na^+ ion screening of anionic functional groups and resulting changes in conformation (Figure 8 a). In the sugar/sugar phosphate region (950−1230 cm^{-1}), there is enhanced intensity at low ionic strength (0−10 mM) of shoulder bands at ca. 1128 and 1028 cm^{-1} and the small band at 979 cm^{-1}, possibly because of diminished interaction of Na^+ with anionic phosphate groups. The broad band centered at 1083 cm^{-1} in pure water is shifted to higher frequency with increasing ionic strength. Prior studies have shown that the stretching vibrations of both charged PO_2^- and ester O−P−O are sensitive to cation interactions.[74] In disodium salt of 2′-deoxyguanosine 5′-monophosphate (Na_2-dGMP), Na^+ ions are in 5- and 6-fold coordination with phosphate groups and water molecules.[75] However, inner-sphere complexation is not required to give such spectral changes; in aqueous systems, similar shift and broadening of mononucleotide phosphate vibrations was attributed to outer-sphere cation coordination.[76]

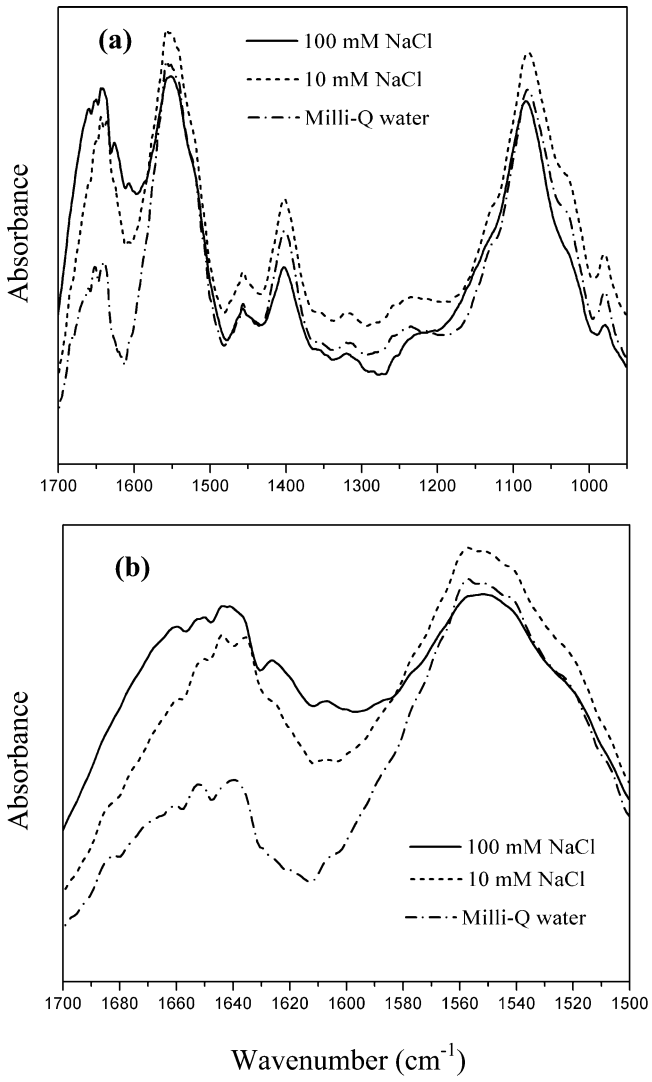

Figure 8. Effect of ionic strength on ATR-FTIR spectra of EPS (free/stationary growth phase): (a) 1800−950 cm^{-1} and (b) 1800−1500 cm^{-1} (10 mg EPS mL^{-1}, 10 and 100 mM NaCl, pH 6.0).

Increasing ionic strength at pH 6 results in an increase in the amide I/amide II band intensity ratio (Figure 8a) from

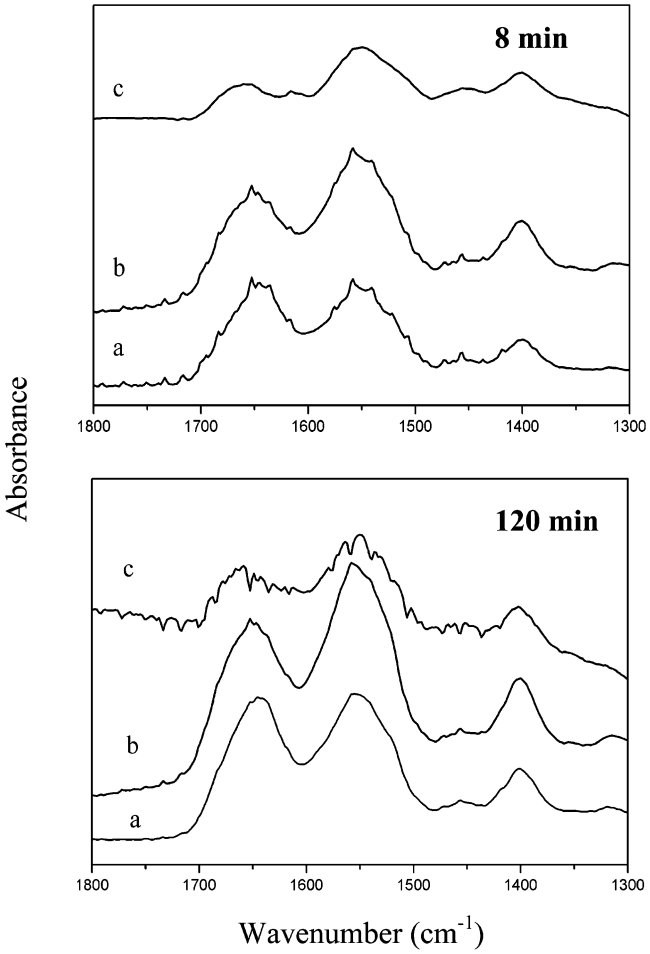

Figure 9. Time dependent ATR-FTIR spectra (1800−1300 cm^{-1}) of (a) solution-phase EPS (uncoated Ge crystal), (b) goethite-adsorbed EPS, and (c) silica-adsorbed EPS (0.0125 g goethite; 0.0125 g silica, 17.9 mg EPS mL^{-1}, 10 mM NaCl, pH 6.0).

0.48 (pure water) to 0.78 (10 mM) to 0.90 (100 mM), which likely reflects a change in protein secondary structure.[77] Second derivative analysis of the amide I band peak locations (Figure 8b) indicates a mixture of α-helical (1652 cm^{-1}) and random coil conformation (1641 cm^{-1}) in pure water. Random coil (1644 cm^{-1}) conformation predominates at 10 mM, whereas further increase in ionic strength to 100 mM yields bands associated with β-turn or β-sheet structures (1661 and 1626 cm^{-1}).

EPS-Mineral Interaction. ATR-FTIR spectra were collected to evaluate EPS interaction with goethite (α-FeOOH) and amorphous silica (SiO_2 am) surfaces in 10 mM NaCl at pH 6. At this pH, the goethite surface is positively charged due to proton complexation at weakly acidic surface hydroxyl groups, whereas silica is negatively charged because of progressive proton dissociation of more strongly acidic silanol sites at pH > 2.5.[10] Identical measurements were collected in the absence of mineral colloids (i.e., solution phase spectra). Interfacial reactions are emphasized when colloidal films are present because of the much larger specific surface area relative to the Ge IRE alone.[78] Spectra of goethite- and silica-sorbed EPS were obtained by subtracting the corresponding colloidal film spectrum (including electrolyte).

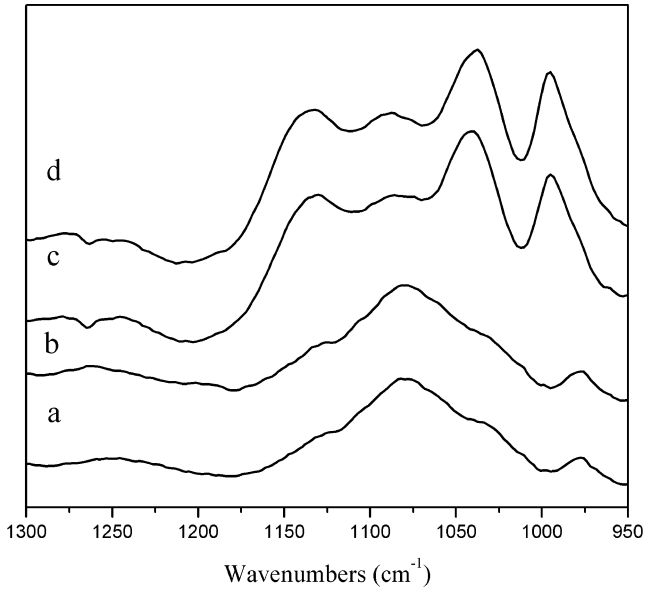

Figure 10. ATR-FTIR spectra (1300−950 cm^{-1}) of (a) solution-phase EPS (8 min), (b) solution-phase EPS (120 min), (c) goethite-adsorbed EPS (8 min), and goethite-adsorbed EPS (120 min) (0.0125 g goethite; 0.0125 g silica, 17.9 mg EPS mL^{-1}, 10 mM NaCl, pH 6.0).

Figure 9 shows ATR spectra (1800−1300 cm^{-1}) of EPS in solution (a), sorbed to goethite (b), and sorbed to silica (c) after 8 and 120 min reaction time. The signal-to-noise ratio increased with time for solution and goethite (indicating accumulation at the interface) but decreased for silica. This difference may be attributed to an initial EPS displacement of silica particles from the negatively charged IRE surface after injection of EPS solution followed by sedimentation of the silica particles and a corresponding time-dependent increase in the Si−O stretch. A similar effect was observed by Mercier and Savoie,[79] and like them, we also observed a corresponding time-dependent increase in the Si−O stretch (not shown), which is consistent with this process.

Adsorption of EPS constituents resulted in an amide I band shift for goethite (from 1642 ± 1 to 1652 ± 2 cm^{-1}) and for silica (from 1642 cm^{-1} to 1662 cm^{-1}). These frequency shifts suggest a preference, upon adsorption, for α-helix structures in goethite and either β-turns or β-sheet structures in silica, relative to the solution phase EPS, where the random coil structure predominates. We also observed differences in the intensity and area ratios of amide I/amide II bands between adsorbed and solution-phase EPS. Several reports have shown that such changes reflect adsorption-induced variation in protein secondary and tertiary structure.[77,80−83] Amide I/amide II peak area ratios calculated from the spectra in Figure 9 (120 min) are 0.99, 0.71, and 0.57 for solution-phase, goethite-adsorbed, and silica-adsorbed EPS, respectively, clearly indicating a change in protein conformation and/or composition upon adsorption. It has been suggested that increasing amide I/amide II peak area ratio for a single type of protein indicates increasing quantity of α-helix structure,[82−83] but such a correlation is not likely applicable to a macromolecular mixture such as EPS, where preferential adsorption of particular components is expected. Indeed, an objective of future research is to assess the extent to which

variation in amide I/amide II band intensity ratios reflects sorptive fractionation versus conformational change of EPS proteins.

In the region 1300−950 cm^{-1}, which is characteristic of vibrations associated with polysaccharides, distinct bands located at 1132, 1088, 1041, and 994 cm^{-1} were clearly evident in all spectra of goethite-sorbed EPS, whereas solution phase EPS exhibits a broad band of overlapping peaks centered at 1082 ± 2 cm^{-1} and a small band at 978 ± 2 cm^{-1} (Figure 10). These results are consistent with preferential adsorption to goethite of particular polysaccharide constituents that bind to surface metals via complexation at acidic functional groups. Chemical interactions between EPS functional groups and the Fe atoms on the goethite surface could involve carboxylic groups on polysaccharides or phosphodiesters on the backbone of nucleic acids (phosphate-sugar). Inner-sphere complexation of carboxylate groups with Fe centers has been observed during sorptive interaction of organic acids with Fe oxides.[84−85] Such binding is reflected in a shift to lower frequency of the asymmetric carboxylate stretching band and enhancement of the symmetric stretch, neither of which were observed in the present study (Figure 9). Rather, the results suggest phosphodiester binding to goethite. Phosphodiester groups of nucleic acids are strongly acidic and dissociate at pH > 3.2 to give univalent negative charge.[86] Bands at 950−1000 cm^{-1} have been attributed to stretching modes of P−OH and P−O−Fe bonds.[87] We attribute the bands at 1132 and 1088 cm^{-1} to P−O stretching and those at 1041 and 994 cm^{-1} to P−O−Fe stretching,[87,88] which suggests that specific adsorption of nucleic acids plays an important role in EPS adsorption to Fe oxide surfaces.

The time-dependent increase in the Si−O stretching vibration (1200−1000 cm^{-1}) hindered our ability to extract IR data from this region of the EPS-silica spectrum (symmetric phosphate stretch of nucleic acid and C−O stretching modes of sugar/sugar phosphate), as has been reported elsewhere.[79,88−89] Variation in intensity and shape of the strong Si−O stretching vibration depends on factors such as size distribution of the silica particles, particle packing after sedimentation from aqueous suspension, and proximity of the particles to the IRE surface.[79]

Conclusions

Under the growth conditions employed in the present study, *B. subtilis* was found to produce a small amount of capsular or cell-bound EPS and a relatively large amount of exudates or free EPS. Growth phase of the bacterium (exponential or stationary) and form of EPS (cell-bound or free) affect the relative proportions of polysaccharide or protein constituents and associated functional group chemistry. Spectroscopic data indicate that free EPS is enriched in carbohydrates during exponential growth and in proteins during stationary growth.

Proton complexation and dissociation at acidic functional groups influences conformational behavior of EPS constituents that are detectable by ATR−FTIR, and the changes are most apparent for EPS proteins. Protein α-helical conformation was observed at pH 2.6/pD ≤ 3 (amide I/I′ bands between 1660 and 1650 cm^{-1}) and random coil (unordered) conformation was observed at high pH/pD ≥ 6 (amide I/I′ bands between 1650 and 1640 cm^{-1}) implying that pH changes in the range of natural waters can affect secondary structure of protein components. IR spectra of mineral-adsorbed EPS indicate that goethite exhibits a greater affinity for EPS constituents than does silica and that the goethite-EPS interaction is mediated by formation of P−O−Fe bonds, whereas a contribution of carboxylate groups to the adsorption process was not evident. The chemical properties of this surface active film likely play an important role in metal ion complexation, bacterial adhesion, and biofilm formation.

Acknowledgment. We thank Dr. Raina Maier and Julie Neilson for assistance with microbial growth studies and Paul Lee and Dr. Ken Nebesny for help with the XPS characterization. This research was supported by the National Science Foundation (NSF) CRAEMS program (Grant CHE-0089156).

References and Notes

(1) Gannon, J.; Manilal, V. B.; Alexander, M. *Appl. Environ. Microbiol.* **1991**, *57* (1), 190−193.
(2) Gannon, J.; Tan, Y H.; Baveye, P.; Alexander, M. *Appl. Environ. Microbiol.* **1991**, *57* (9), 2497−2501.
(3) Fontes, D. E.; Mills, A. L.; Hornberger, G. M.; Herman, J. S. *Appl. Environ. Microbiol.* **1991**, *57* (9), 2473−2481.
(4) Mills, A. L.; Herman, J. S.; Hornberger, G. M.; Dejesus, T. H. *Appl. Environ. Microbiol.* **1994**, *60* (9), 3300−3306.
(5) Burks, G. A.; Velegol, S. B.; Paramonova, E.; Lindenmuth, B. E.; Feick, J. D.; Logan, B. E. *Langmuir* **2003**, *19* (6), 2366−2371.
(6) Phoenix, V. R.; Martinez, R. E.; Konhauser, K. O.; Ferris, F. G. *Appl. Environ. Microbiol.* **2002**, *68*, 4827−4834.
(7) Doyle, R. J. In *Metal Ions & Bacteria*; Beveridge, T. J., Doyle, R. J., Eds.; Wiley-Interscience: New York, 1989.
(8) Fein, J. B.; Daughney, C. J.; Yee, N.; Davis, T. A. *Geochim. Cosmochim. Acta* **1997**, *61*, 3319−3328
(9) Ferris, F. G.; Beveridge, T. J. Functions of bacterial cell surface structures. *BioScience* **1985**, *35*, 172−177.
(10) Stumm, W. *Chemistry of the Solid-Water Interface: Processes at the Mineral-Water and Particle−Water Interface in Natural Systems*; Wiley: New York, 1992.
(11) Bolster, C. H.; Mills, A. L.; Hornberger, G. M.; Herman, J. S. *J. Contam. Hydrol.* **2001**, *50*, 287−305.
(12) Poortinga, A. T.; Bos, R.; Norde, W.; Busscher, H. J. *Surf. Sci. Rep.* **2002**, *47* (1), 1−32.
(13) Velegol, S. B.; Logan, B. E. *Langmuir* **2002**, *18* (13), 5256−5262.
(14) Camesano, T. A.; Abu-Lail, N. I. *Biomacromolecules* **2002**, *3*, 661−667.
(15) Jayaratne, P.; Keenleyside, W. J.; MacLachlan, P. R.; Dodgson, C.; Whitfield, C. *J. Bacteriol.* **1993**, *175*, 5384−5394.
(16) van Loosdrecht, M. C. M.; Lyklema, J.; Norde, W.; Schraa, G.; Zehnder, A. J. B. Appl. *Environ. Microbiol.* **1987**, *53*, 1893−1897.
(17) van Loosdrecht, M. C. M.; Norde, W.; Lyklema, J.; Zehnder, A. J. B. *Aquat. Sci.* **1990**, *53*, 103−114.
(18) Absoiom, D. R.; Lamberti, F. V.; Policova, Z.; Zingg, W.; Van Oss, D. J.; Neumann, A. W. *Appl. Environ. Microbiol.* **1983**, *46*, 90−97.
(19) Beveridge, T. J.; Fyfe, W. S. *Can. J. Earth Sci.* **1985**, *22*, 1893−1898.
(20) Camesano, T. A.; Logan, B. E. *Environ. Sci. Technol.* **2000**, *34* (16), 3354−3362.
(21) Williams, V.; Fletcher, M. *Appl. Environ. Microbiol*. **1996**, *62*, 100−104.
(22) Doyle, J. R.; Rosenberg, M. *Microbial Cell Surface Hydrophobicity*; American Society of Microbiology: Washington, 1990.
(23) Tadros, T. F. In *Microbial Adhesion to Surfaces*; Berkeley, R. C. W., Lynch, J. M., Melling, J., Rutter, P. R., Vincent, B., Eds.; Ellis Horwood Publishers: Chichester, U.K., 1980.
(24) Beveridge, T. J.; Graham, L. L. *Microbiol. Rev.* **1991**, *55*, 684−705.
(25) Bruno C.; van der, Aa.; Dufrene, Yves F. *Colloids Surf. B: Biointerfaces* **2002**, *23*, 173−182.

(26) Decho, A. W. *Oceanogr. Mar. Biol. Annu. Rev.* **1990**, *28*, 73−153.
(27) Sutherland, I. W. CRC *Crit. Rev. Microbiol.* **1984**, *60*, 434−446.
(28) Veiga, M. C.; Jain, M. K.; Wu, W. W.; Hollingsworth, R. I.; Zeikus, J. G. *Appl. Environ. Microbiol.* **1997**, *63*, 403−407.
(29) Videla, H. A. *Manual of Biocorrosion*; CRC Press: Boca Raton, FL, 1996.
(30) Flemming, H. C. *Chem. Ingnieur Technik.* **1995**, *67*, 1425−1430.
(31) Cheng, S. S.; Chittur, K. K.; Sukenik, C. N.; Culp, L. A.; Lawrence, K. *J. Colloid Interface Sci.* **1994**, *162*, 135−143.
(32) Ong, J. L.; Chittur, K. K.; Lucas, L. C. *J Biomed. Mater. Res.* **1994**, *28*, 1337−1346.
(33) VanHippel, P. H.; Schleich, T. In *Structure and Stability of Biological Macromolecules*; Timasheff, S. N., Fasman, G. D., Eds.; Dekker: New York, 1969.
(34) Tirrell, M. In *Interactions of Surfactants with Polymers and Proteins*; Goddard, E. D., Ananthapadmanabhan, K. P., Eds.; CRC Press: Boca Raton, FL, 1993.
(35) de Brouwer, J. F. C.; Wolfstein, K.; Stal, L. J. *Eur. J. Phycol.* **2002**, *37*(1), 37−44.
(36) Atkinson, R. T.; Posner, A. M.; Quirk, J. P. *J. Phys. Chem.* **1967**, *71*, 550−558.
(37) Glasoe, P. K.; Long, F. A. *J. Phys. Chem.* **1960**, *64*, 188−190.
(38) Dubois, M.; Gilles, K. A.; Hamilton, J. K.; Reber, P. A.; Smith, F. *Anal. Chem.* **1956**, *28*, 350−356.
(39) Lowry, O. H.; Rosebrough, N. J.; Farr, A. L.; Randall, R. J. *J. Biol. Chem.* **1951**, *193*, 265−275.
(40) Cescutti, P.; Toffanin, R.; Pollesello, P.; Sutherland, I. W. *Carbohydr. Res.* **1999**, *31*, 159−168.
(41) Lindsay, P.; Valerie M. H.; Marshall, M. E.; Yucheng, G.; Andrew, P. L. *Carbohydr. Polym.* **1998**, *37*, 123−130.
(42) Tadaya, K.; Tadashi, T.; Akira, T. *J. Chromat. A* **1983**, *256*, 61−69.
(43) Chan, K.; Xu, L.; Fang, H. H. P. *Environ. Sci. Technol.* **2002**, *36*, 1720−1727.
(44) Yan, L.; Marzolin, C.; Terfort, A.; Whitesides, G. M. *Langmuir* **1997**, *13*, 6704−6712.
(45) Chastain, J.; King, R, C., Jr. *Handbook of X-ray Photoelectron Spectroscopy*; Physical Electronics: Eden Prairie, MN, 1995.
(46) Beamson, G.; Briggs, D. *High-Resolution XPS of Organic Polymers*; Wiley: Chichester, U.K., 1992.
(47) Stipp, S. L.; Hochella, M. F., Jr. *Geochim. Cosmochim. Acta* **1991**, *55* (6), 1723−1736.
(48) Bruinsma, G. M.; van der Mei H. C.; Busscher, H. J. *Biomaterials* **2001**, *22* (24), 3217−3224.
(49) Latrache, H.; EL Ghmari, A.; Karroua, M.; Hakkou, A.; AIT Mousse, H.; EL Bouadili, A.; Bpurlioux, P. *Microbiologica* **2002**, *25*, 75−82.
(50) Rouxhet, P. G.; Mozes, N.; Dengis, P. B.; Dufrêne, Y. F.; Gerin, P. A.; Genet, M. *Colloid Surf. B: Biointerfaces* **1994**, *2*(1−3), 347−369.
(51) Udelhoven, T.; Naumann, D.; Schmitt, J. *Appl. Spectrosc.* **2000**, *54*, 1471−1479.
(52) Zeroual, W.; Choisy, C.; Doglia, S M.; Bobichon, H.; Angiboust, J. F.; Manfait, M. *Biochim. Biophys., Acta* **1999**, *1222*, 171−178.
(53) Helm, D.; Naumann, D. *FEMS Microbiol. Lett.* **1995**, *126*, 75−80.
(54) Schmitt, J.; Flemming, H. *Int. Biodeterior. Biodegrad.* **1998**, *41* (1), 1−11.
(55) Hubner, W.; Blume, A. *Chem. Phys. Lipids* **1998**, *96* (1−2), 99−123.
(56) Hoekstra, F. A.; Wolkers, W. F.; Buitink, J.; Golovina, E. A.; Crowe, J. H.; Crowe, L. M. *Comp. Biochem. Physiol.* **1997**, *117A* (3), 335−341.
(57) Hadzi, D.; Hodoscek, M.; Grdadolnik, J.; Avbelj, F. *J. Mol. Struct.* **1992**, *266*, 9−19.
(58) Nara, M.; Tasumi, M.; Tanokura, M.; Hiraoki, T.; Yazawa, M.; Tsutsumi, A. *FEBS Lett.* **1994**, *349*, 84−88.
(59) Laberge, J. M.; Wright, W. W.; Sudhakar, S.; Liebman, P. A.; Vanderkooi, J. M. *Biochemistry* **1997**, *36*, 5363−5371.
(60) Barja, B. C.; Herszage, J.; Alfonso, M. D. *Polyhedron* **2001**, *20* (15−16), 1821−1830.
(61) Barja, B. C.; Afonso, M. S. *Environ. Sci. Technol.* **1998**, *32*, 3331−3335.
(62) Tejedor-Tejedor, M. I.; Anderson, M. A. *Langmuir* **1990**, *6* (3), 602−611.
(63) Casal, H. L.; Mantsch, H. H. *Biochim. Biophys. Acta* **1984**, *779*, 381−401.
(64) Castillo, E. J.; Koenig, J. L.; Anderson, J. M.; Lo, *J. Biomater.* **1984**, *5*, 319−325.
(65) Jung, C. *J. Mol. Recognit.* **2000**, *13* (6), 325−351.
(66) Joachim A.; Hering, J. A.; Innocent, P. R.; Harris, P. I. *Proteomics* **2002**, *2*, 839−849.
(67) van de Weert, M.; Haris, P. I.; Hennink, W. E.; Crommelin, D. J. A. *Anal. Biochem.* **2001**, *297* (2), 160−169.
(68) Cantor, C. R.; Schimmel, P. R. *Biophysical Chemistry*; W. H. Freeman and Company: New York, 1980.
(69) Buijs, J.; Norde, W.; Lichtenbelt, J. W. Th. *Langmuir* **1996**, *12*, 1605−1613.
(70) Susi, H.; Byler, D. M. *Biopolymers* **1986**, *25*, 469−487.
(71) Krimm, S.; Bandekar, J. *Adv. Protein Chem.* **1986**, *38*, 181−364.
(72) Surewicz, W. K.; Mantsch, H. H.; Chapman, D. *Biochemistry* **1993**, *32* (2), 389−394.
(73) Surewicz, W. K.; Mantsch, H. H. *Biochim. Biophys. Acta (BBA)−Protein Struct. Mol. Enzymol.* **1988**, *952*, 115−130.
(74) Grdadolnik, J.; Hadzi, D. *Chem. Phys. Lipids* **1993**, *65*, 121−132.
(75) Young, D. W.; Touline, P.; Wilson, H. R. *Acta Crystallogr. B* **1974**, *30*, 2012−2018.
(76) Nafisi, Sh.; Mohajerani, N.; Hadjiakhoondi, A.; Monajemi, M.; Garib, F. *J. Mol. Struct.* **2001**, *562*, 35−43.
(77) Ishida, K. P.; Griffiths, P. R. *Appl. Spectrosc.* **1993**, *47*, 584−589.
(78) McQuillan, A. J. *Adv. Mater.* **2001**, *13* (12−13), 1034−1038.
(79) Mercier, P.; Savoie, R. *Biospectroscopy* **1997**, *3* (4), 299−306.
(80) Lenk, T. J.; Ratner, B. D.; Gendreau, R. M.; Chittur, K. K. *J. Biomed. Mater. Res.* **1989**, *23*, 549−569.
(81) Wasacz, F. M.; Olinger, J. M.; Jakobsen, R. J. *Biochem.* **1987**, *26*, 1464−1470.
(82) Kato, K.; Matsui, T.; Tanaka, S. *Appl. Spectrosc.* **1987**, *41*, 861−865.
(83) Giacomelli, C. E.; Maria, G. E.; Bremer, G.; Norde, W. *J. Colloid Interface Sci.* **1999**, *220*, 13−23.
(84) Duckworth, O. W.; Martin, S. T. *Geochim. Cosmochim. Acta* **2001**, *65* (23), 4289−4301.
(85) Chorover, J.; Amistadi, M. K. *Geochim. Cosmochim. Acta* **2001**, *65* (1), 95−109.
(86) Martinez, D. S.; Smith, R. E.; Kulczycki, E.; Ferris, F. G. *J. Colloid Interface Sci.* **2002**, *253*, 130−139.
(87) Sheals, J.; Sjoberg, S.; Persson, P. *Environ. Sci. Technol.* **2002**, *36*, 3090−3095.
(88) Gong, W. *Int. J. Miner. Process* **2001**, *63*, 47−165.
(89) Mao, Y. N.; Daniel, L. N.; Whittaker, N.; Saffiotti, U. *Environ. Health Perspect.* **1994**, *102*, 1−15.

BM034461Z